Optimum Two-Impulse Orbital Transfer and Rendezvous between Inclined Elliptical Orbits

GARY A. MCCUE*
North American Aviation Inc., Downey, Calif.

Mathematical formulations of the general—inclined orbits and free end points—optimum two-impulse orbital transfer problem lead to expressions that, except for special cases, are analytically intractable. Numerical techniques were developed and used to study optimum transfer modes; many orbit pairs yield four useful relative optima. A parameter space was adopted to represent the impulse function; that is, impulse is a function of takeoff point, arrival point, and transfer orbit semilatus rectum. This abstraction allowed visualization and detailed examination of surfaces of constant impulse, thus revealing the structure of the impulse function. As a result of this study, one may predict the gross properties of "impulse function spaces" and consequently determine the optimum two-impulse orbital transfer circumstances for any pair of elliptical orbits. The entire procedure of impulse optimization, requiring less than 1 min of IBM 7090 time, is accomplished for free end points; i.e., impulse is minimized with respect to takeoff and arrival points, as well as transfer orbit geometry. The method easily is extended to computation of time constraints for two-impulse rendezvous. An approximation to optimum two-impulse rendezvous when time constraints are specified is also explored.

Nomenclature

a	=	semimajor axis
e	=	eccentricity (magnitude of e)
i	=	inclination
p	=	semilatus rectum
r	=	magnitude of satellite's position vector
t	=	time
$\Delta\theta$	=	transfer angle (true anomaly difference in transfer orbit plane)
τ	=	relative phase between vehicles; rendezvous time constraint
μ	=	gravitation constant
ϕ_1	=	angle from reference axis to departure position in initial orbit
ϕ_2	=	angle from reference axis to arrival position in terminal orbit
ω	=	argument of perigee; angle from reference axis to perigee point
Ω	=	right ascension of ascending node
$\mathbf{e}$	=	orbit shape and orientation vector
$\mathbf{I}$	=	impulse vector
$\mathbf{N}$	=	unit vector denoting reference direction (line of intersection of initial and final orbit planes)
$\mathbf{r}$	=	geocentric satellite position vector
$\mathbf{U}_1$	=	unit vector directed toward point of departure from initial orbit
$\mathbf{U}_2$	=	unit vector directed toward point of arrival in final orbit
$\mathbf{V}$	=	velocity vector
$\mathbf{W}$	=	unit vector directed along orbit's angular momentum vector
$\boldsymbol{\phi}$	=	independent variable vector (ϕ_1, ϕ_2, p)
$\mathbf{N}\,\mathbf{M}\,\mathbf{W}_2$	=	orthogonal unit vector set that establishes reference coordinate system

I. Introduction

SUCCESS of a variety of space missions depends ultimately upon an ability to maneuver in orbit. The high fuel requirements usually associated with orbit-changing maneuvers make it essential that optimum orbital transfer modes be investigated—optimum in the sense of minimum fuel requirements. Although these modes might not be employed in the actual mission, they do represent lower bounds against which vehicle design compromises may be measured.

This paper concerns optimum two-impulse orbital transfer and rendezvous between any pair of unperturbed elliptical orbits. The objective of the orbital transfer maneuver is to transform the five orbital elements p, e, ω, i, Ω of an initial orbit to match corresponding elements of a final orbit. This is accomplished by instantaneous velocity changes (impulses) that may be applied at arbitrary points on the initial and final orbits. Impulse optimization is accomplished for *free end points;* i.e., impulse is minimized with respect to takeoff and arrival points, as well as transfer orbit geometry. The term rendezvous is used to imply an additional constraint to the two-impulse orbital transfer process—that of physically meeting a vehicle in the final orbit.

Little analytic information is known about the optimum orbital transfer when end points are unspecified. Like many problems of celestial mechanics, the formulation is straightforward, and, except for special cases, the equations are analytically intractable. Thus, for the general problems, one accepts simplifications in the mathematical model or uses numerical techniques.

Numerical methods were employed to allow visualization of an "impulse function space," a geometrical abstraction of the impulse function. This technique allowed concise graphical presentation of all optimum impulse information concerning any pair of elliptical orbits. As a result, it was possible to understand the nature and structure of the entire impulse function.

II. Two-Impulse Orbital Transfer Formulation

This study involves a two-impulse transfer process between an initial orbit with elements p_1, e_1, ω_1, i_1, and a final orbit with elements p_2, e_2, ω_2 (Fig. 1). The formulation assumes Keplerian orbits and results from choosing the final orbit as the reference plane ($i_2 = 0$); i_1 is the relative inclination of the two orbit planes ($\cos i_1 = \mathbf{W}_1 \cdot \mathbf{W}_2$, where $\mathbf{W}_1$ and $\mathbf{W}_2$ are unit vectors directed along the angular momentum vectors of the initial and final orbits). For coplanar orbits, the refer-

Received January 21, 1963; revision received May 23, 1963. The studies presented here constitute an extension of work performed for Marshall Space Flight Center under Contract NAS8-1582 (Satellite Rendezvous Study).

* Research Scientist, Space Sciences Laboratory, Space and Information Systems Division. Member AIAA.

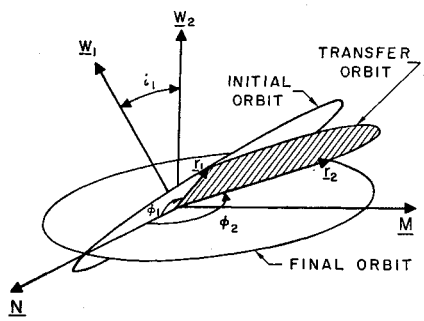

Fig. 1 Transfer geometry.

ence direction (**N**) is arbitrary, but for inclined orbits, **N** is defined as the line of intersection of the two orbit planes ($\mathbf{N} = \mathbf{W}_2 \times \mathbf{W}_1/|\mathbf{W}_2 \times \mathbf{W}_1|$).

For the general case, there is a three-parameter family of transfer orbits joining any two specific orbits. The objective of this study was to select transfer orbits that minimized the sum of the two velocity increments required to perform the transfer. Optimization was accomplished by numerical means, a fact that has an important bearing on the choice of independent variables. The angles from the reference line to departure point (ϕ_1) and to arrival point (ϕ_2) are a natural choice for two of the three optimizing variables, since they, along with the given orbital elements, specify position and velocity in the known orbits (Fig. 1). Furthermore, except for the special case when the arrival and departure points are colinear with the center of mass, ϕ_1 and ϕ_2 establish the plane of the transfer orbit.

The third independent variable must be one of the elements of the transfer orbit: p, e, or ω. The semilatus rectum p of the transfer orbit was the third parameter used for this study. It was chosen since it simplified the structure of the impulse function $I(\phi) = I(\phi_1, \phi_2, p)$. It also avoided several undesirable discontinuities that are present in other formulations. (A discussion of the use of alternate variables may be found in Refs. 1 and 2.)

Transfer Geometry

Unit vectors ($\mathbf{U}_1$, $\mathbf{U}_2$) and radius vectors ($\mathbf{r}_1$, $\mathbf{r}_2$) toward the departure and arrival points may be computed from ϕ_1, ϕ_2 and the elements of the initial and final orbits:†

$$\mathbf{U}_1 = (\cos\phi_1, \sin\phi_1 \cos i_1, \sin\phi_1 \sin i_1) \quad (1)$$

$$\mathbf{U}_2 = (\cos\phi_2, \sin\phi_2, 0) \quad (2)$$

$$\mathbf{r}_j = \left[\frac{p_j}{1 + e_j \cos(\phi_j - \omega_j)}\right] \mathbf{U}_j \qquad j = 1,2 \quad (3)$$

Unit vectors normal to the initial, final, and transfer orbit planes are defined as follows:

$$\mathbf{W}_1 = (0, -\sin i_1, \cos i_1) \quad (4)$$

$$\mathbf{W}_2 = (0, 0, 1) \quad (5)$$

$$\mathbf{W}_t = \mathbf{U}_1 \times \mathbf{U}_2/|\mathbf{U}_1 \times \mathbf{U}_2| \qquad \mathbf{U}_1 \times \mathbf{U}_2 \neq 0 \quad (6)$$

Two vectors that define the shape and orientation of the initial and final orbits complete the transfer geometry description (this formulation has been suggested by Herget[4]):

$$\mathbf{e}_j = e_j[\cos\omega_j, \sin\omega_j \cos i_j, \sin\omega_j \sin i_j] \qquad j = 1,2 \quad (7)$$

The true anomaly interval traversed in the transfer orbit ($\Delta\theta$) may be determined directly:

$$\cos\Delta\theta = (\mathbf{U}_1 \cdot \mathbf{U}_2) \qquad 0° < \Delta\theta < 180° \quad (8)$$

† The subscripts 1, 2, and t indicate initial, final, and transfer orbits. Lack of a subscript also is employed to denote a transfer orbit parameter.

Note that $\Delta\theta$ is arbitrarily limited to the first two quadrants ("short" transfers). A reversal of the algebraic signs of the transfer orbit velocity vectors is employed to compute "long" transfer circumstances. For elliptical transfer orbits, optimum impulse is defined as the least of the optimum long and short transfer impulses. Note that this particular formulation is singular if $\Delta\theta = 180°$ or $\Delta\theta = 0°$. For these cases, the impulse required is not unique, since any transfer orbit inclination will satisfy the geometry. In many special cases the optima occur when $\Delta\theta = 180°$, and an alternate set of computations is necessary to avoid this singularity.

Impulse Computation

The function to be minimized is the total impulse for the two-impulse maneuver:

$$I = |\mathbf{I}_1| + |\mathbf{I}_2| \quad (9)$$

where

$$I_1 = \pm\mathbf{V}_{t_1} - \mathbf{V}_1 \quad (10)$$

$$I_2 = \mathbf{V}_2 \mp \mathbf{V}_{t_2} \quad (11)$$

(When a double sign is used, the upper sign refers to the short transfer case.) Velocity vectors in the initial and final orbits at the departure and arrival points ($\mathbf{V}_1$ and $\mathbf{V}_2$) and the corresponding velocity vectors in the transfer orbit ($\mathbf{V}_{t_1}$ and $\mathbf{V}_{t_2}$) are computed as follows:

$$\mathbf{V}_j = (\mu/p_j)^{1/2}\mathbf{W}_j \times (\mathbf{e}_j + \mathbf{U}_j) \qquad j = 1,2 \quad (12)$$

$$\mathbf{V}_{tj} = (\mu/p)^{1/2}\mathbf{W}_t \times (\mathbf{e} + \mathbf{U}_j) \qquad j = 1,2 \quad (13)$$

Equations (12) and (13) may be derived from Eq. 3.26 of Herget.[4] An expression for **e** is not included, since this transfer orbit parameter is not required in the final equations for impulse computation. The final impulse equations are obtained from Eqs. (10–13) by substituting Eq. (6) and performing several algebraic manipulations:

$$\mathbf{I}_1 = \pm[\mathbf{v} + z\mathbf{U}_1] - \mathbf{V}_1 \quad (14)$$

$$\mathbf{I}_2 = \mathbf{V}_2 \mp [\mathbf{v} - z\mathbf{U}_2] \quad (15)$$

where

$$\mathbf{v} = [(\mu p)^{1/2}(\mathbf{r}_2 - \mathbf{r}_1)]/|\mathbf{r}_1 \times \mathbf{r}_2| \quad (16)$$

$$z = (\mu/p)^{1/2} \tan(\Delta\theta/2) \quad (17)$$

Impulses corresponding to long and short transfers are compared, and the combination producing the lesser impulse is used for the remaining optimization procedures.

III. Impulse Function Investigation

Although the formulation of the expressions for impulse computation is relatively straightforward, the exact mathematical expressions are not susceptible to analytical solution. One must, therefore, resort to numerical techniques for optimizing the solution vector, $I(\phi) = I(\phi_1, \phi_2, p)$.

At best, conventional numerical search techniques only provide information concerning a function's local properties. Yet, a detailed understanding of the impulse function's structure is essential for interpretation of numerical results. The number, shape, and relative importance of minima are requisite to a complete analysis of transfer problems, since numerical optimization methods (e.g., steepest descent) find only that minimum impulse which is closest to the point of search initiation.[2, 3]

A geometric ("ϕ-space") representation of the impulse function was adopted for this investigation. In Fig. 2, p, ϕ_1, and ϕ_2 are measured along the principal axes of an orthogonal coordinate system. All possible transfers between a pair of orbits (excluding the $\Delta\theta = 0°$ and $\Delta\theta = 180°$ function singularities) lie within the volume defined by $0° \leq \phi_1 <$

$360°, 0° \leq \phi_2 < 360°, 0 < p < +\infty$. Of course, ϕ_1 and ϕ_2 undergo cyclical repetition outside this volume.

Studying the impulse function in ϕ-space requires visualization of surfaces that are the loci of points having the same impulse. These "impulse surfaces" are generally closed and surround optima in much the same manner that the successive layers of an onion enclose its center. Impulse surfaces may be visualized and studied by considering their traces upon a cutting plane (Fig. 2). The resulting contours of equivalent impulse that appear in most of the figures presented here will be shown to provide a wealth of data in a concise, easily understood form.

These contour maps are produced from an array of impulse values that are parametrically generated from Eq. (9), with ϕ_1, ϕ_2, or p being held constant. Constant impulse contour lines, consisting of short straight-line segments, then are fitted between the survey points. It is important to note that the fidelity of the contouring technique depends directly upon the number of survey points. This fact should be remembered when examining certain structural details of the figures presented here.

Several seconds of IBM 7090 time are required to contour a typical array of survey data (500 to 1000 points). A Stromberg Carlson 4020 CRT then is employed to plot the contour maps. A description of the contouring technique appears in Ref. 5.

Hohmann Transfer ϕ-Space

Figure 3 was produced by cutting the ϕ-space associated with coplanar circular orbits having $p_1 = 5000$ and $p_2 = 6000$ miles. Cutting planes corresponded to $\phi_2 = 0°$ and $p = 5454.54$ miles. In this case, the symmetry is so complete that an adequate description of the ϕ-space is possible with the two contour maps presented. Symmetry about the $\phi_1 - \phi_2 = 180°$ plane is apparent. The Hohmann transfer corresponds to the straight line $\phi = (\phi_1, \phi_1 + 180°, p)$ with ϕ_1 arbitrary and $p = 5454.54$ miles. All other impulse surfaces are cylinders having elements parallel to the Hohmann line minimum. In Fig. 3, the minimum impulse contour corresponds to 2500 fps.

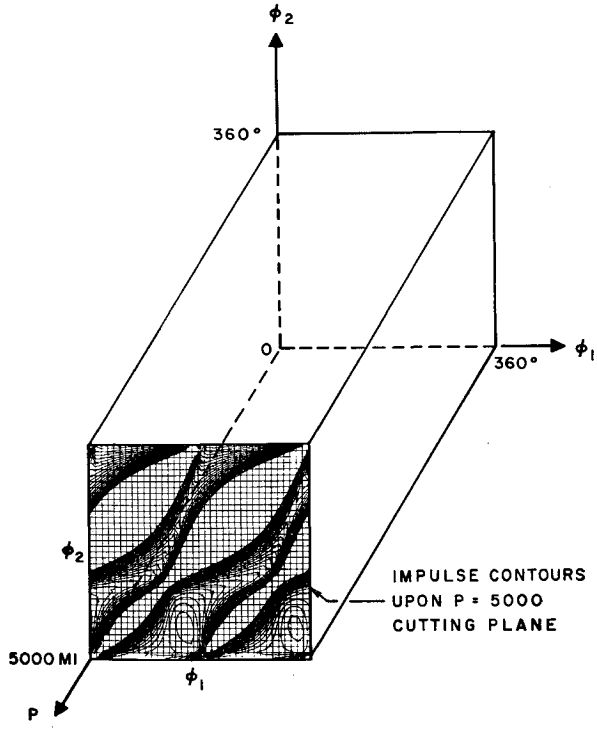

Fig. 2 Schematic view of impulse function space and impulse contours.

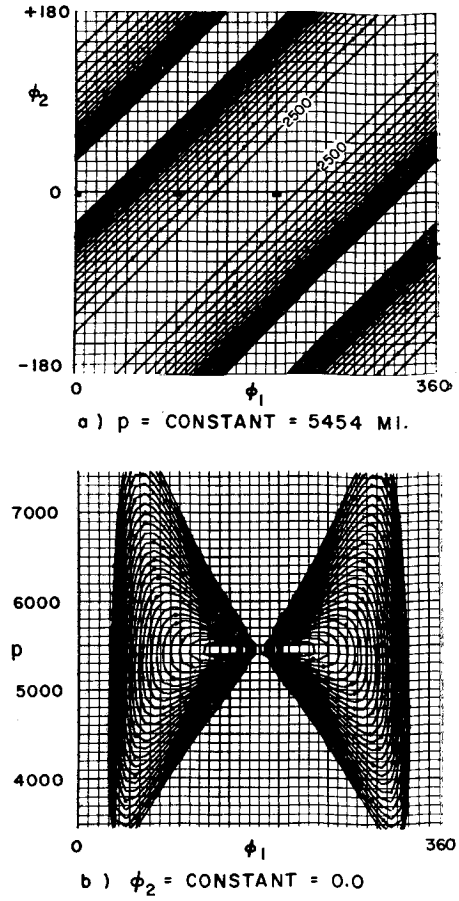

Fig. 3 Impulse contours for coplanar circular orbits (contour interval = 500 fps).

Inclined Asymmetric Orbit Pair

Figure 4 concerns an orbit pair having the following elements: $p_1 = 5000$ miles, $p_2 = 6000$ miles, $e_1 = 0.2$, $e_2 = 0.2$, $\omega_1 = -90°$, $\omega_2 = +30°$, and $i_1 = 5°$.

The five p = const contour maps presented here adequately illustrate the ϕ-space associated with a typical unsimplified problem. The perfect symmetry and simplicity of the circle-to-circle case is in sharp contrast with the seemingly amorphous impulse contours of asymmetrical cases. The shapes and relative orientations of the two orbits are apparent from the illustration that projects the initial orbit upon the final orbit plane.

The existence of four distinct relative optimum transfers between these two orbits is apparent. The approximate coordinates and impulse associated with each of the optima are summarized in Table 1. Uncontoured portions of each survey plane correspond to hyperbolic and elliptical transfer orbits that require excessive impulses.

IV. p-Optimization

The technique of passing a number of cutting planes through a given ϕ-space suffices to isolate optima and other pertinent features. However, as a ϕ-space becomes more complex, this technique requires that numerous contour maps be generated, each of them providing additional information concerning the optimum transfer modes.

A "p-optimization" technique was developed to overcome these difficulties and thus present one contour map containing only optimum impulse information.

Given ϕ_1 and ϕ_2 (i.e., $\mathbf{r}_1$ and $\mathbf{r}_2$), it is desired to find that p which minimizes the impulse defined by Eq. (9). Differentiating Eq. (9) yields

$$dI = [(\mathbf{I}_1 \cdot d\mathbf{I}_1)/|\mathbf{I}_1|] + [(\mathbf{I}_2 \cdot d\mathbf{I}_2)/|\mathbf{I}_2|] \qquad (18)$$

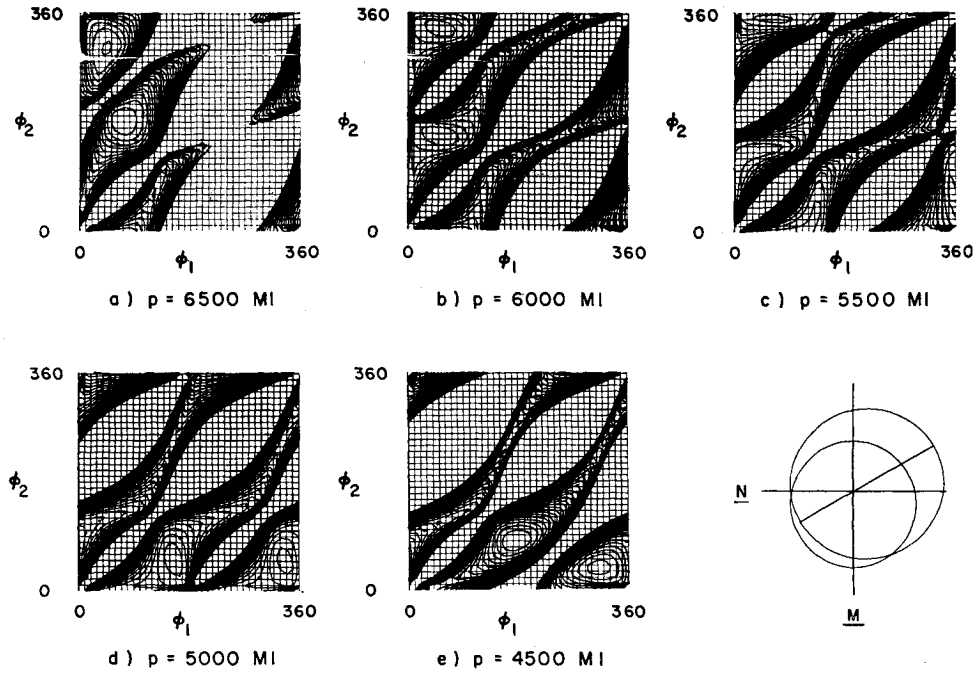

Fig. 4 Inclined asymmetric orbit pair; impulse contours for p = constant planes (contour interval = 500 fps).

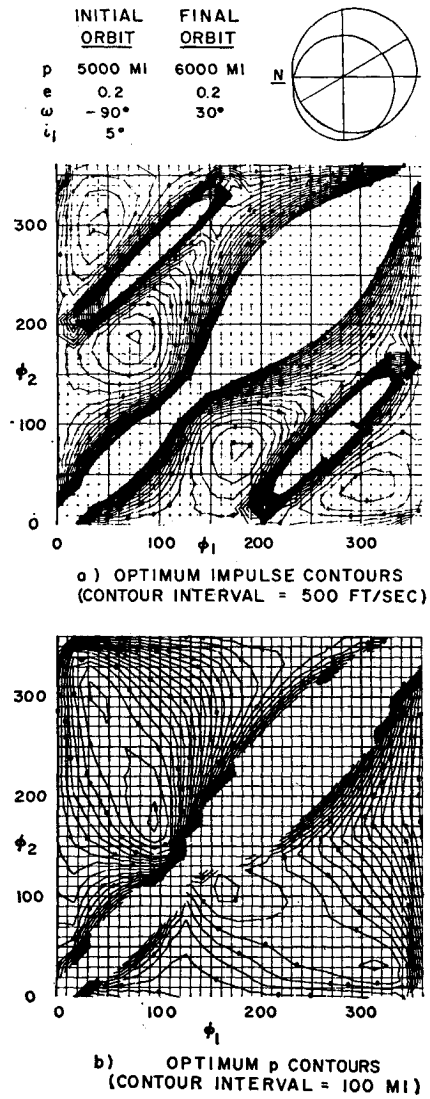

Fig. 5 Inclined asymmetric orbit pair.

Since $\mathbf{V}_1$ and $\mathbf{V}_2$ are independent of p,

$$\partial \mathbf{I}_1/\partial p = \pm(\partial \mathbf{V}_{t_1}/\partial p) \tag{19}$$

$$\partial \mathbf{I}_2/\partial p = \mp(\partial \mathbf{V}_{t_2}/\partial p) \tag{20}$$

This leads to an expression for the derivative of impulse with respect to p, which may be set equal to zero:

$$\frac{\partial I}{\partial p} = \pm \frac{1}{2p}\left[\frac{\mathbf{I}_1\cdot(\mathbf{v} - z\mathbf{U}_1)}{|\mathbf{I}_1|} - \frac{\mathbf{I}_2\cdot(\mathbf{v} + z\mathbf{U}_2)}{|\mathbf{I}_2|}\right] = 0 \tag{21}$$

Equation (21) is used to direct a numerical search that seeks the value of p which minimizes impulse for the given ϕ_1 and ϕ_2. Though Eq. (21) has several roots, usually only those roots which correspond to elliptical transfer orbits are useful for impulse minimization. For certain elliptical orbit pairs, it can be shown that optimum two-impulse transfers between particular groups of end points result in hyperbolic transfer orbits.[6] The range of p which produces an elliptical transfer orbit is bounded. These boundaries (parabolic orbit limits) are defined as follows:

$$p_{\min} = \frac{r_1 r_2 - \mathbf{r}_1\cdot\mathbf{r}_2}{r_1 + r_2 + [2(r_1 r_2 + \mathbf{r}_1\cdot\mathbf{r}_2)]^{1/2}} \tag{22}$$

$$p_{\max} = \frac{r_1 r_2 - \mathbf{r}_1\cdot\mathbf{r}_2}{r_1 + r_2 - [2(r_1 r_2 + \mathbf{r}_1\cdot\mathbf{r}_2)]^{1/2}} \tag{23}$$

Except for certain special cases, only one minimum impulse will occur between these limits.[6] An effective numerical technique has been devised to seek the required optimum impulse solutions where $p_{\min} < p < p_{\max}$. Each determination of an optimum p requires less than 0.1 sec of IBM 7090 time.

The contour maps presented throughout the remainder of this paper were generated using this technique. Approximately 500 p-optimizations were required for the generation of each contour map.

Table 1 Identification of optima

Optimum	ϕ_1	ϕ_2	p, miles	Impulse, fps
1	75°	190°	6650	4900
2	40°	300°	6600	5300
3	175°	75°	4600	5400
4	310°	40°	4600	5800

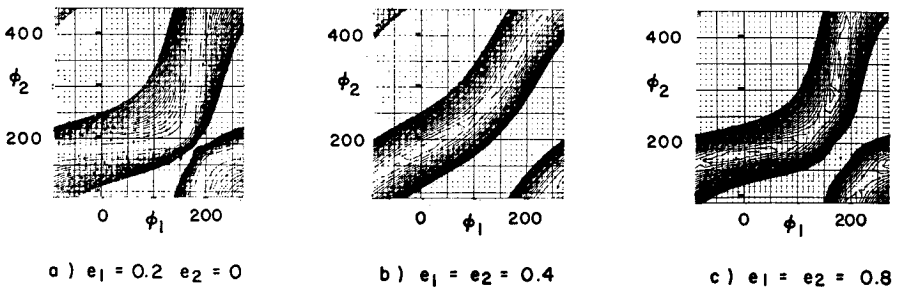

Fig. 6 Effect of eccentricity addition; coplanar coapsidal orbits (contour interval = 200 fps).

Figure 5a is a p-optimized survey of the ϕ-space associated with the orbit pair that was examined in Fig. 4. Note that the optimum impulse (feet per second) for any ϕ_1, ϕ_2 may be read directly from the contour map. The advantages of the p-optimization technique should be apparent from a comparison of Figs. 4 and 5a. Complete description of a ϕ-space requires the generation of numerous cuts at various values of one of the variables. Once these cuts are available, it is difficult to extract the optimum impulse information. The p-optimization technique allows complete description of the optimum impulse regions of a ϕ-space in one contour map.

Another contour map (Fig. 5b) presents the p contours associated with the optimum impulse contours. The optimum p associated with any ϕ_1, ϕ_2 is, therefore, available. One may proceed easily from these contour maps to numerical searching programs that permit exact detailed examination of regions of particular interest.[2]

Note that Fig. 5 readily illustrates the circumstances of the four optimum transfers. At the same time, it is possible to note their relative importance and to infer certain other properties, such as error sensitivity, i.e., $\partial I/\partial\phi_1$ and $\partial I/\partial\phi_2$ may be approximated from the contour maps. Other features of ϕ-space structure, such as regions of extreme impulse, are apparent. The nature and properties of these features were the subject of considerable investigation.

The entire computational procedure necessary to produce Figs. 5a and 5b required less than 1 min of IBM 7090 time.

V. Formation of Local Optima

This study resulted in the identification of mechanisms that guide the formation of optima and determine their multiplicity. It was found that the number, shape, and distribution of minima of the impulse function are controlled by the type of asymmetries present in the given orbit pair. Eccentricity, inclination, and the relative position of the lines of apsides all have distinct effects upon the structure of function space.

Effect of Eccentricity Perturbations

The first orbit pair of Fig. 6 represents a transfer from an elliptical orbit ($e_1 = 0.2$, $p_1 = 5000$ miles) to a circular orbit ($p_2 = 6400$ miles). The Hohmann optimum region of the circle-to-circle case has been twisted into nearly horizontal and vertical optimum regions. The optimum transfer occurs at $\phi = (0°, 180°, p_{opt})$,[7] but near optimum transfers are available throughout the entire range of ϕ_1. The strong warping of the impulse contours is associated with the varying radial distances separating the two orbits.

Addition of sufficient eccentricity ($e_1 = e_2 = 0.4$, $p_1 = 5000$ miles, $p_2 = 6000$ miles) to allow the orbits to intersect under the proper rotations disturbs the Hohmann line optimum and forms two distinct optima[5] at $\phi = (0°, 180°, p_{opt})$ and $\phi = (180°, 0°, p_{opt})$. As additional eccentricity ($e_1 = e_2 = 0.8$, $p_1 = 5000$ miles, $p_2 = 6000$ miles) is added; the optima become more pronounced and are separated by a larger impulse differential. If the orbits are coapsidal, the optima always correspond to perigee-to-apogee and apogee-to-perigee transfers.

Coplanar Rotation of Lines of Apsides

When coplanar elliptical orbits ($e_1 = e_2 = 0.2$, $p_1 = 5000$ miles, $p_2 = 6000$ miles) are rotated, a new type of optimum modifying asymmetry is introduced (Fig. 7). As the orbits approach tangency, the optimum impulse contours are bent into one section that is nearly horizontal and another that

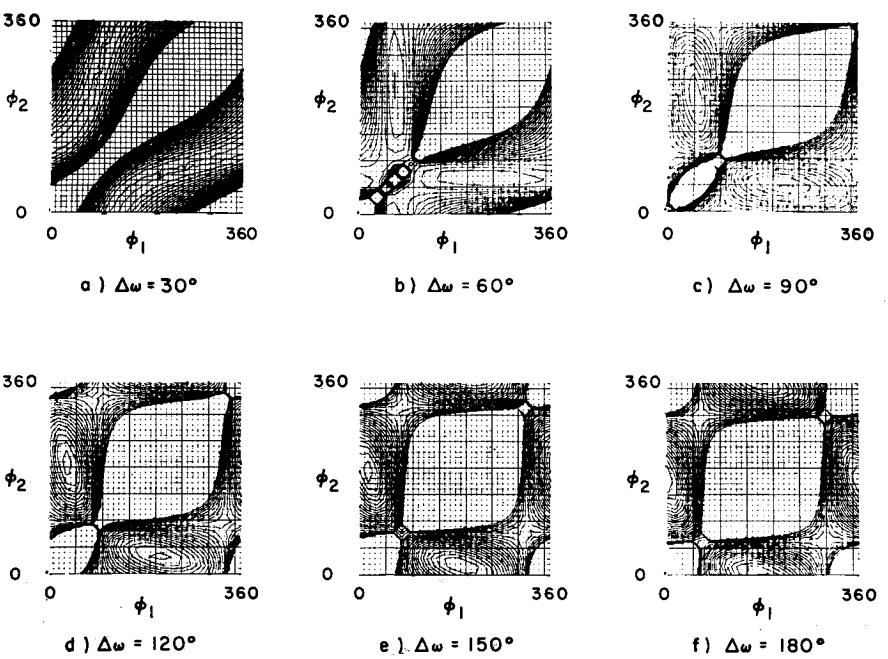

Fig. 7 Effect of coplanar rotation of elliptical orbits (contour interval = 200 fps).

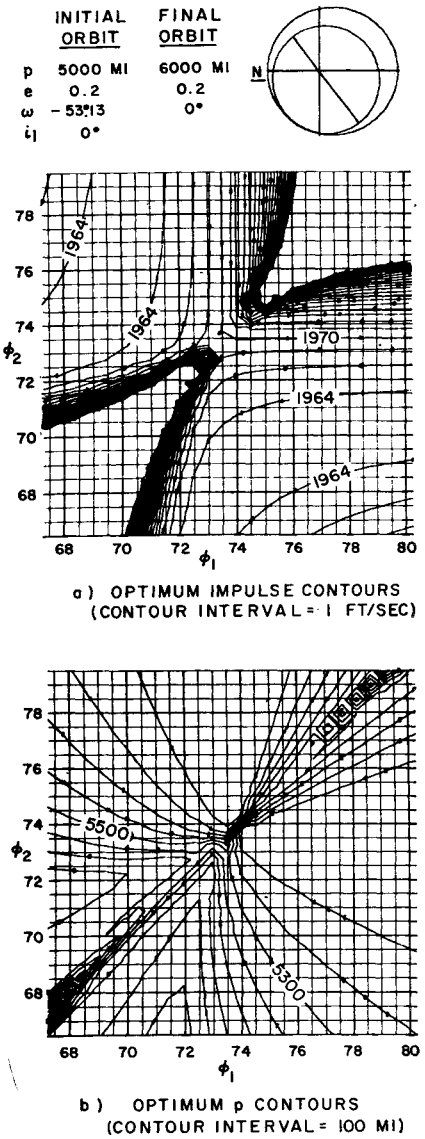

Fig. 8 Tangent elliptical orbits.

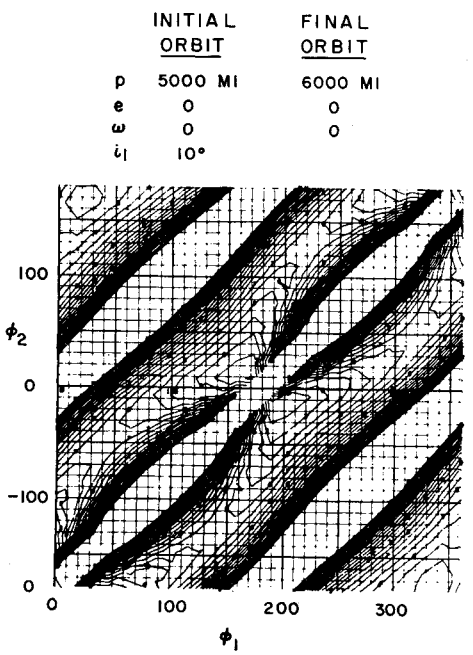

Fig. 9 Inclined circular orbits (contour interval = 500 fps).

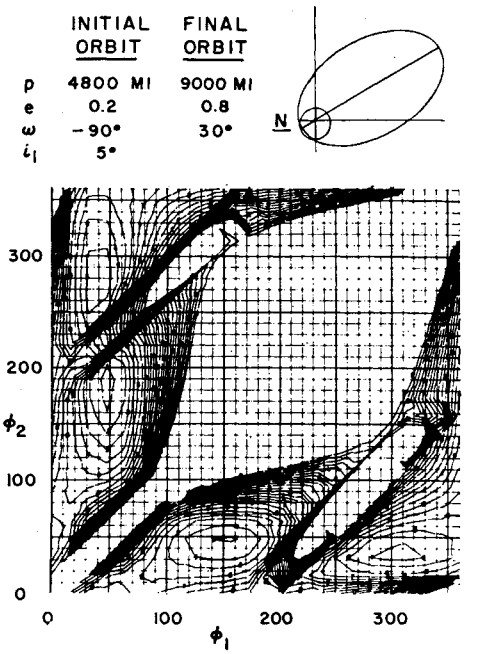

Fig. 10 Inclined elliptical orbits (contour interval = 500 fps).

is nearly vertical ($\Delta\omega = 30°$). The optima migrate to locations adjacent to the coordinates of the point at which the orbits would become tangent under further rotation. Further rotation ($\Delta\omega = 60°$) causes the orbits to intersect and the optima to shift from near the tangency point to the horizontal and vertical regions mentioned earlier. These regions correspond to transfers that use most of the total impulse at either the departure or the arrival point; a single impulse transfer is possible if the orbits are tangent or intersecting.

Further rotation causes the two optima to become less elongated, to correspond to greater minimum impulse levels, and to migrate toward $\phi = (0°, 180°, p_{opt})$ and $\phi = (180°, 0°, p_{opt})$. The uncontoured regions indicate the excessive impulse that is required to transfer via high-eccentricity orbits that pass near the center of mass.

Tangent Orbits

When coplanar orbits are tangent and also coapsidal, it can be shown that a one-impulse transfer at the point of tangency is optimum. However, if the orbits have undergone coplanar rotation, this is no longer true.[7]

Figures 8a and 8b present the impulse and p contours that result from a pair of tangent orbits. The impulse for the one-impulse transfer $I(\phi) = I(73°.74, 73°.74, 6000)$ is about 1971.3 fps. Two seemingly symmetrical regions corresponding to impulse levels of about 1963 fps are centered near $\phi = (74°, 68°, p_{opt})$ and $\phi = (68°, 74°, p_{opt})$. A quick glance at the p contours associated with these optima (Fig. 8b) indicates that a transfer orbit semilatus rectum of about 5400 miles is optimum (note that $p_1 = 5000$ miles and $p_2 = 6000$ miles). This result indicates that approximately equal initial and final impulses will produce the optimum transfer.

Inclination

Inclination produces a division of a given ϕ-space about the $\phi_1 - \phi_2 = 180°$ plane (Fig. 9). In this case two circular orbits are inclined 10°. Contours appear to radiate from the $\phi = (0°, 180°, p_{opt})$ and $\phi = (180°, 0°, p_{opt})$ points which are singularities in the impulse computation formulation. These points are optima if the orbits are inclined about their semimajor axes, but for other orientations the optima may

lie elsewhere. Increasing the inclination causes the ϕ-space division to become more pronounced.

All ϕ-spaces resulting from inclined orbits exhibit an inclination "wall," which, in general, tends to double the number of optima which would have existed if the orbits had been coplanar. For instance, Fig. 5 results from adding inclination to a pair of elliptical orbits whose lines of apsides are separated by 120°.

VI. Additional ϕ-Space Studies

Space does not permit the comprehensive examination of enough ϕ-spaces to develop a complete picture of the optimum orbital transfer circumstances that arise from all possible orbit combinations. Figures 10 and 11 are presented to answer several additional questions and, no doubt, to raise several more.

The asymmetrical orbit pair that produced Fig. 5 was altered to produce Figs. 10 and 11 (10: $p_1 = 4800$ miles, $p_2 = 9000$ mile, $e_2 = 0.8$, 11: $p_1 = 4800$ miles, $p_2 = 7920$ miles). The first pair of orbits can intersect under appropriate rotations. Even though the final orbit is considerably enlarged relative to the initial, the ϕ-space structure remains similar to that of Fig. 5. The dominant role of orbit orientation is apparent from this illustration.

The nonintersecting orbit pair (Fig. 11) exhibits only two optima, although the orbit orientations are identical. This example illustrates how the number of optima is multiplied when orbits are capable of intersection.

VII. Two-Impulse Rendezvous

An optimum two-impulse orbital transfer is also an optimum rendezvous for two vehicles with an appropriate phase relationship. The foremention orbital transfer techniques may be extended easily to allow calculation of rendezvous time constraints for arbitrary ϕ_1, ϕ_2, and p.

In order to define a time constraint, let zero time correspond to the arrival of a vehicle in the final orbit at the reference line (N), and let τ be the time at which the vehicle in the initial orbit will cross the same reference. If t_1, t_2, and t_t are the traverse times associated with the true anomaly intervals ϕ_1, ϕ_2, and $\Delta\theta$, then a sufficient condition for rendezvous

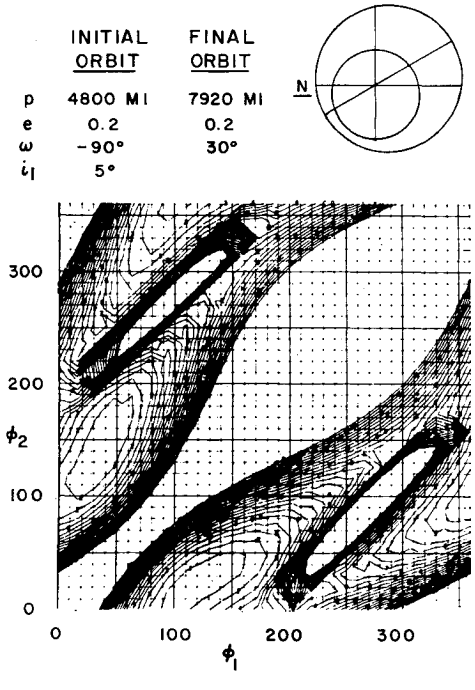

Fig. 11 Nonintersecting elliptical orbits (contour interval = 500 fps).

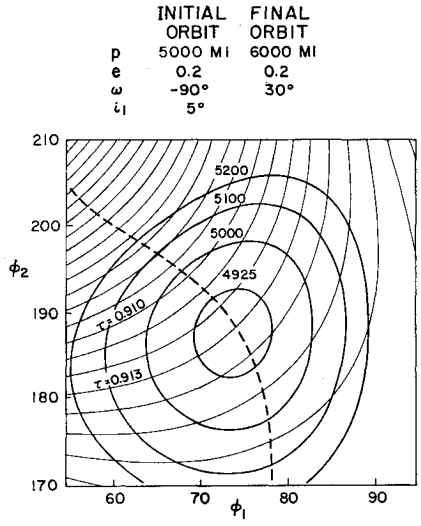

Fig. 12 Optimum impulse and corresponding τ contours near principal optimum.

is that $t_1 + t_t = t_2 - \tau$. Expressing τ in units of the final orbit's period (T_2) yields

$$\tau = (t_2 - t_1 - t_t)/T_2 \tag{24}$$

Using Kepler's equation, it is a simple matter to compute $\tau(\phi) = \tau(\phi_1, \phi_2, p_{opt})$. Therefore, the values of τ associated with the p-optimized impulse also may be contoured. Figure 12 superimposes the p-optimized impulse and corresponding τ contours associated with the principal optimum of Fig. 5. Clearly, τ must equal 0.913 for the optimum impulse rendezvous.

Of course, it will be a rare instance when τ is such that the optimum impulse rendezvous may be accomplished during a given revolution. Fortunately, for nonsynchronous orbits τ changes each revolution, and a near optimum value eventually will result. An impulse-splitting technique that is detailed in Ref. 1 may be used to achieve a three-impulse rendezvous that requires no more impulse than the optinum two-impulse orbital transfer.‡ One may, therefore, avoid waiting a prolonged period in order to achieve the optimum impulse rendezvous.

When τ is specified, impulse optimization requires finding ϕ_1, ϕ_2, and p such that the impulse and τ surfaces are tangent. Numerical search techniques, such as steepest descent, have been employed to seek the required solutions.[1, 8] Experience has demonstrated that economical and effective use of these numerical search methods requires adequate knowledge of a function's properties. With this knowledge, it is possible to determine initial conditions that will assure rapid convergence to the required relative optimum.

Figure 12 allows one to approximate the conditions required for an optimum time constrained rendezvous. Given τ, one may locate the position where the corresponding τ line approaches nearest to the impulse optimum. (The locus of these positions is shown as a dashed line.) The ϕ_1, ϕ_2, and p located by this process usually will not yield an optimum time constrained rendezvous. Note, however, that the optimum impulse must be less than or equal to this approximate value. Therefore, the method provides a convenient means for determining whether the impulse required for rendezvous is within vehicle system capabilities. The method also provides information concerning the behavior of the impulse and τ functions. This information allows a good choice of initial conditions for subsequent investigation of exact solutions by other numerical procedures.

‡ Reference 1 uses a τ that is the negative of the τ employed here.

VIII. Conclusion

Methods for systematically studying optimum two-impulse orbital transfer between any pair of elliptical orbits have been developed and used to investigate the properties of an "impulse function space." The mechanisms that govern the structure of this function space have been determined and may be employed now to predict the optimum transfers resulting from any pair of elliptical orbits.

A contouring technique was used to present large amounts of optimum impulse information in a concise, easily understood form. The results obtained from function contouring have been verified through the use of steepest descent optimization procedures.[2,8] Initial conditions taken from the contour maps always allowed the numerical search program to converge to the proper local optimum within a few seconds of IBM 7090 time. Optimum impulses obtained from this exact numerical optimization were only slightly better than those obtained from contouring. In all instances where exact numerical solutions were required, the insight gained through contouring methods proved to be an invaluable aid to subsequent optimization by conventional techniques.

Although the methods presented here are oriented principally toward the area of space mission design, they also provide numerous clues that point the way to analytical solution of numerous subproblems.

References

[1] Des Jardins, P. R., Bender, D. F., and McCue, G. A., "Orbital transfer and satellite rendezvous," SID 62-870, North American Aviation Inc. (August 31, 1962).

[2] Kerfoot, H. P., Bender, D. F., and Des Jardins, P. R., "Analytical study of satellite rendezvous (final report)," MD 59-272, North American Aviation Inc. (October 20, 1960).

[3] Des Jardins, P. R. and Bender, D. F., "Extended satellite rendezvous study (quarterly report, 31 May through 31 August 1961)," SID 61-304, North American Aviation Inc. (September 14, 1961).

[4] Herget, P., *The Computation of Orbits* (published privately by the author, Ann Arbor, Mich., 1948), p. 30.

[5] McCue, G. A., "Optimization by function contouring techniques," SID 63-171, North American Aviation Inc. (February 10, 1963).

[6] Bell, H. W. and Lee, B. G., "Analysis of two-impulse orbital transfer," unpublished private communication (1963).

[7] Ting, L., "Optimum orbital transfer by impulses," ARS J. **30**, 1013–1018 (1960).

[8] Des Jardins, P. R. and Bender, D. F., "Extended satellite rendezvous study (quarterly report, 31 August through 30 November 1961)," SID 61-459, North American Aviation Inc. (December 15, 1961).

AUGUST 1963 AIAA JOURNAL VOL. 1, NO. 8

Effect of an Oblate Rotating Atmosphere on the Eccentricity, Semimajor Axis, and Period of a Close Earth Satellite

FORD KALIL*
The Martin Company, Baltimore, Md.

Expressions are derived for the secular effects of a rotating atmosphere on the eccentricity of a close earth satellite for $0 \leq e \leq 0.01$. Two cases were considered: 1) the atmosphere is spherical and its density varies exponentially with altitude; and 2) the atmosphere is oblate, has the same flattening as the earth, and varies exponentially with altitude. In both cases, the atmosphere was assumed to rotate with the same angular velocity as the earth. In addition, expressions are derived for the secular effects of the oblate rotating atmosphere on the semimajor axis and period for $0 \leq e \leq 0.01$. Variations in air density, such as diurnal or seasonal variations, were neglected. It was found that both the rotation of the atmosphere and its oblateness significantly affect the eccentricity, semimajor axis, and period over one revolution. The expressions derived are accurate for the cases being considered and can be used for accurate atmospheric density interpretations based on known satellite motions or for accurate predictions of satellite motion and position. The modified Bessel functions of the first kind are used extensively in this report. Hence, for purposes of completeness, they are tabulated up to the eighth order for an argument of 0 through 2.

Nomenclature

a = semimajor axis
A = satellite cross-sectional area
$A_0, A_1, A_2, A_3, A_4, A_5$ = quantities which are defined in Eqs. (75–80)
B = ballistic coefficient = $C_D A/2m$
$B_0, B_1, B_2, B_3, B_4, B_5$ = quantities defined in Eqs. (94–99)
c = $K a e$
C_D = aerodynamic drag coefficient
d = $(\Omega_e/n)(1 - e^2)^{1/2} \cos i$
D_S = radial component of drag force per unit mass
D_T = component of drag force per unit mass perpendicular to the radius vector
D_W = component of drag force per unit mass normal to the orbital plane
$\mathbf{D}$ = $-B\rho v^2 \hat{v}$ = aerodynamic drag force per unit mass due to air resistance
e = orbital eccentricity
E = eccentric anomaly
f = earth's flattening = 1/298.3
h = altitude above the surface of a spheroidal earth; also the aereal constant
h_π = altitude at perigee

Received by ARS October 17, 1962. The author wishes to express his gratitude to Fred Martikan for his many helpful suggestions and comments.

* Senior Engineering Specialist, Aerospace Mechanics Department; now with NASA Goddard Space Flight Center, Greenbelt, Md.